Basic Research on Inverse Design for Seismic-isolated and Response-controlled Structures

Ippei HATA[1], Shinji ISHIMARU[2] and Takeshi FURUHASHI[3]

[1] *Assistant Engineer, College of Science and Technology, Nihon Univ., Tokyo, Japan*
[2] *Professor, Dept. of Architecture, College of Science and Technology, Nihon Univ., Tokyo, Japan*
[3] *Associate Professor, Dept. of Architecture, College of Science and Technology, Nihon Univ., Tokyo, Japan*
Email: ippei.hata@nihon-u.ac.jp, ishimaru@arch.cst.nihon-u.ac.jp, furuhashi@arch.cst.nihon-u.ac.jp

ABSTRACT:

This paper presents an inverse design method of SDOF structures through performance-based diagrams which can easily estimate the suitable design parameters for various dampers to satisfy the target design performances to be specified for a given earthquake ground motion. The diagrams are constructed based on the concept of separated variables of the energy spectrum. The concept is in engineering sense that a response energy spectrum of a nonlinear structure subjected to a given ground motion $S_{eq}\{S(T),h_0,\mu_V,p_V,\mu_d,p_d\}$ can be expressed by the product between the corresponding elastic response spectrum $S(T)$ and the empirical formulas $\tau(h_0,\mu_V,p_V,\mu_d,p_d)$. The formulas are derived by the statistic for the results of the time history simulations over a great number of earthquake ground motions, in which the adopted variables are viscous damping ratios, ductility factors, bilinear coefficients, relief velocity ratios and bilinear viscous coefficient ratios, etc. The accuracy of the parameters estimated by the performance-based diagrams is verified by a number of time history simulations.

KEYWORDS: separate variables of energy spectrum, performance-based diagrams, response spectrum, elasto-plastic damper, bilinear type oil damper

1. INTRODUCTION

Recent developments in passively-controlled structures in Japan have led to a new seismic design method in which response values can be controlled by increasing the energy dissipation capacities of structures through various devices such as oil dampers and elasto-plastic dampers, etc [1-5]. In addition, global environmental issues prompt the establishment of a design method for super long-life structures. That is, even if they are subjected to severe ground motions, any structural element remains undamaged by absorbing almost of the vibration energy through damper systems, and then changing the fatigued dampers due to the severe earthquake with new devices. As a result, the structure can be resuscitated with the initially specified seismic performance. However, it is very difficult to assess seismic performance in applying inelastic time history analysis, because of the excessive combination of parameters to be taken into account, for example, combinations including natural period T, ductility factors μ_d, bilinear coefficients p_d for elasto-plastic dampers and viscous damping ratios h_0, relief velocity ratios μ_V, and bilinear viscous coefficient ratios p_V for nonlinear viscous dampers, etc. Hence, this paper presents an inverse design method for SDOF structures through seismic performance-based diagrams which can easily estimate the suitable design parameters for various dampers to satisfy the target design performances to be specified for a given earthquake ground motion. The diagrams are constructed based on the concept of separated variables of the energy spectrum. The concept is in engineering sense that a response energy spectrum for a nonlinear structure against a ground motion $S_{eq}\{S(T),h_0,\mu_V,p_V,\mu_d,p_d\}$ can be expressed by the product between the corresponding elastic response spectrum $S(T)$ and the empirical formulas $\tau(h_0,\mu_V,p_V,\mu_d,p_d)$. Since the evaluation of response velocities and displacements are required in designing oil dampers and elasto-plastic dampers, the energy concept including both values is adopted accordingly. That is, there is no way but to estimate the vibration energy of the system from the viewpoint that the dampers are installed to absorb the vibration energy. A study of the separate variables of the energy spectrum was first carried out by S. Ishimaru for the structure systems with elasto-plastic dampers and linear oil dampers [4,5]. This paper presents improved performance-based diagrams, based on Ishimaru's method, for systems with elasto-plastic dampers and bilinear-type oil dampers.

2. CONSTRUCTION OF PERFORMANCE BASED DIAGRAM

2.1. Modified viscosity energy and modified strain energy

The following is an outline of the process to obtain the seismic performance-based design diagrams for systems with bilinear-type viscous damper and bilinear-type elasto-plastic damper.
At the first step, assume the natural period $T_E\left(=2\pi/\omega_0\right)$ and viscous damping ratio $h_0\left(=c_0/\left(2\omega_0 m\right)\right)$ of the system with bilinear hysteretic restoring force characteristics having bilinear coefficient p_d as shown in Fig. 1. Then, the target ductility factor μ_d and the relief velocity ratio μ_V are specified for a given earthquake ground motion.
Next, a sequence of time history analyses are repeated in order to obtain the parameters which satisfy the target ductility factor μ_d and the relief velocity ratio μ_V of the system, where the symbols are illustrated in Fig. 2.
After repeating the time history simulations, we obtain the velocity $V_{y,h}$ satisfying the target relief velocity ratio μ_V and the yield deformation $x_{e,d}$ satisfying the target ductility factor μ_d [7]. Consequently, for the relationships between the damping force and deformation of a non-linear damper shown in Fig. 3(a), the dissipation energy due to viscous damping E_h is obtained by Eq. (2) [6].

$$\mu_V = \frac{V_{max}}{V_{y,h}} \qquad (1)$$

$$E_h = \pi c_0 V_{max} D_{max}\left[1+\frac{2(1-p_V)}{\pi}\left\{\frac{\sqrt{\mu_V^2-1}}{\mu_V^2}-cos^{-1}\left(\frac{1}{\mu_V}\right)\right\}\right] \qquad (2)$$

$$E_{Bi,h} = \frac{1}{2}E_h \qquad (3)$$

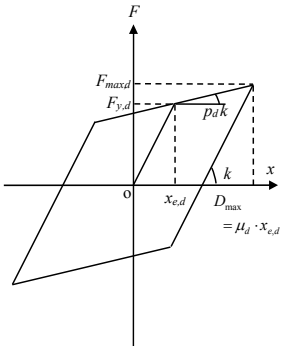

Fig.1. hysteretic characteristics

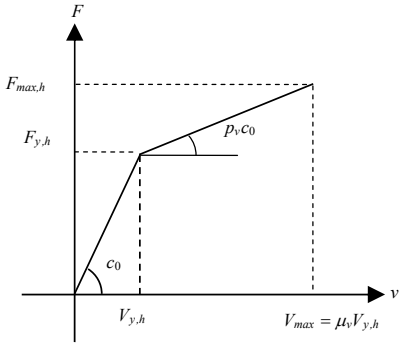

Fig. 2. Damping force-velocity relationship

Where the symbol $E_{Bi,h}$ represents the area in the hatched part in Fig. 3(a), named as the modified viscosity energy of viscous damper.
For the elasto-plastic damper, the modified strain energy E_d is defined by Eq. (4) for the hatched part of Fig. 3(b) [4,5].

$$E_{Bi,d} = \frac{1}{2}k^2 x_{e,d}\left\{6(\mu_d-1)(1-p_d)+p_d\left(\mu_d{}^2-1\right)+1\right\} \qquad (4)$$

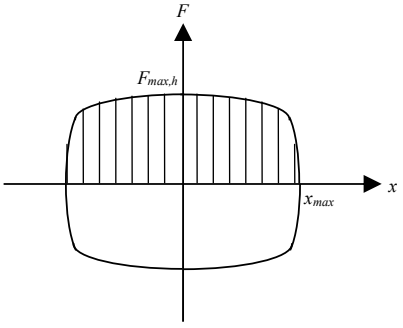

Fig.3(a). Model of modified viscosity energy

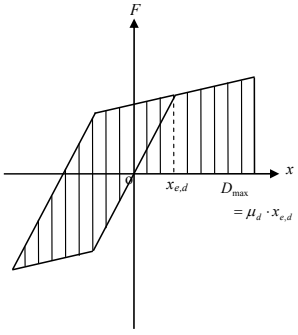

Fig.3(b). Model of modified strain energy

As mentioned later, the effective natural period T' as the elongation of the period due to the plastic behavior of the system is defined as follows [4, 5].

$$T' = T_E\left[1+\sqrt{\frac{\mu_d}{1+p_d(\mu_d-1)}}-\sqrt{\frac{2}{1+p_d}}\right] \quad \mu_d \geqq 3, \qquad T' = T_E\left[0.155\left\{\frac{\mu_d}{1+p_d(\mu_d-1)}\right\}+0.845\right] \quad \mu_d \leqq 3 \qquad (5)$$

The formations for the modified energies and the effective natural period are determined with intuitive models to make the concept of separated variables of energy spectrum maintain through a number of trial and error cycles [4,5].
Thus, the maximum pseudo velocity $\hat{V}_{max}$ is defined by Eq. (6), in which ω' is the effective circular frequency. Eq. (3) is rewritten accordingly by Eq. (7).

$$\hat{V}_{\max} = \omega' \cdot D_{\max} \qquad (6) \qquad E'_{Bi,h} = \frac{1}{2}\pi c_0 \hat{V}_{\max} D_{\max}\left[1+\frac{2(1-p_V)}{\pi}\left\{\frac{\sqrt{\mu_V{}^2-1}}{\mu_V{}^2}-\cos^{-1}\left(\frac{1}{\mu_V}\right)\right\}\right] \qquad (7)$$

Then, the total modified energy E is obtained by the sum of both the modified energies in Eqs. (4) and (7). Hence, the equivalent velocity spectra S_{Bi} are defined by Eq. (11).

$$E = E'_{Bi,h} + E_{Bi,d} \qquad (8) \qquad \frac{1}{2}mS_{Bi}{}^2 = E \qquad (9) \qquad \frac{k_0}{m} = \omega_0^2 \ , \ \frac{c}{m} = 2h_0\omega_0 \qquad (10)$$

$$S_{Bi}{}^2(T_E) = \omega_0^2 x_{e,d}{}^2\left\{6(\mu_d-1)(1-p_d)+p_d(\mu_d{}^2-1)+1\right\}+\pi\, 2h_0\omega_0\omega' D_{\max}{}^2\left[1+\frac{2(1-p_V)}{\pi}\left\{\frac{\sqrt{\mu_V{}^2-1}}{\mu_V{}^2}-\cos^{-1}\left(\frac{1}{\mu_V}\right)\right\}\right] \qquad (11)$$

2. 2 Separated variables of energy spectrum

First, the pseudo velocity spectrum $pS_{V,40}$ and the velocity spectrum $S_{V,40}$ are adopted as the design spectra of the system with viscous damping ratio 0.40, in which the pseudo velocity is derived by multiplying the maximum response displacement to the corresponding natural circular frequency ω_0.
Next, the equivalent velocity spectra S_{Bi} are calculated for the parameters shown in Table. 1.
Each spectrum analysis is carried out for 22 SDOF systems with the period range from 0.4 to 4.0 s, which are chosen as control points for each response spectrum.
In addition, an ensemble of 50 earthquake records listed in Table. 2 is selected to cover a variety of earthquake magnitudes, peak ground motion parameters, recording-site characteristics, geographic locations, and so forth.
Fig. 4(a), for the 1940 El Centro N-S record, shows the $pS_{V,40}(T_E)$ spectrum and a group of $S_{Bi}(T_E)$ spectra for the structures with damping ratio h_0=0.20, relief velocity ratio μ_V=4.0, p_V=0.20 and p_d=0.10. They are plotted for every ductility factor specified from 3.0 to 50.0. The ratios of $pS_{V,40}(T_E)$ to $S_{Bi}(T_E)$ are also plotted in the figure.

Table 1. List of specified parameters

ductility factor μ_d	3, 5, 7.5, 10, 15, 20, 30, 50
bilinear coefficient p_d	0.05, 0.1, 0.2, 0.4
viscous damping ratio h_0	0.1, 0.2, 0.3, 0.4
relief velocity ratio μ_v	1, 2, 4, 7.5, 10
bilinear viscous coefficient ratio p_v	0.1, 0.2, 0.3, 0.4, 1

$$\kappa_{40}(h_0, \mu_V, p_V, \mu_d, p_d) = \frac{S_{Bi}(T')}{pS_{V,40}(T_E)} \fallingdotseq \text{constant} \qquad (12)$$

Table 2. List of earthquake records

Earthquake	Date	Numbers computed here
Imperial Valley	1940/5/18	2
Kern Country	1952/7/21	2
Tokachi-Oki	1968/5/16	2
San Fernando	1971/2/09	4
Miyagiken-Oki	1978/6/12	4
Hyogo-Ken Nannbu	1995/1/17	12
Tottori-Ken Seibu	2000/10/06	6
Geiyo	2001/03/24	4
Miyagiken-Oki	2003/05/26	4
Tokachi-Oki	2003/09/26	6
Niigata-Ken Chubu	2004/10/23	4
Σ		50

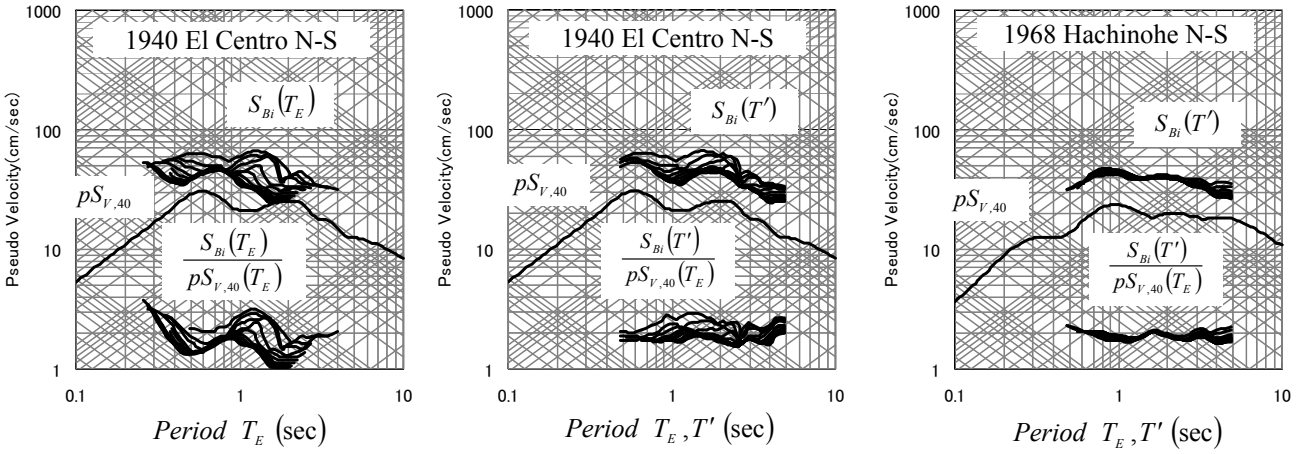

Fig .4 (a) Comparisons between $pS_{V,40}(T_E)$ and $S_{Bi}(T_E)$. Both spectra are plotted along the initial natural period T_E .(b) Comparisons between $pS_{V,40}(T_E)$ and $S_{Bi}(T')$ to be plotted along the effective natural period T'

Fig .5 Comparisons between $pS_{V,40}(T_E)$ and $S_{Bi}(T')$ to be plotted along the effective natural period T'

It is observed that even if the initial periods of the structures are the same, the values of $S_{Bi}(T_E)$ vary significantly from each other depending on the specified ductility factors.
Shifting these spectra in the direction of longer periods along the period axis according to the magnitude of each specified ductility factor, however, reveals that the spectra have similar configurations. This means that the earthquake input energy to the system depends mainly on the effective natural period T' according to the magnitude of elasto-plastic deformations caused in the structure. In other words, the effective natural period T' of Eq. (5) is found out to make the relationships of Eq. (12) maintain as mentioned before.
Fig. 4(b) shows $pS_{V,40}(T_E)$ and a set of $S_{Bi}(T')$ shifting the spectra $S_{Bi}(T_E)$ toward longer periods according to the effective natural period T'. The relationships of Eq. (12) can be confirmed in engineering sense. The same relations can be also observed for other earthquake records listed in Table. 2, as shown in an example of Fig. 5. As a result, we can define the new function $\kappa_{40}(h_0, \mu_V, p_V, \mu_d, p_d)$ expressed by Eq. (12) which does not contain the periodic function T .
Thus, after obtaining the numerical values of $\kappa_{40}(h_0, \mu_V, p_V, \mu_d, p_d)$ to all data of Table. 2, the constants of the empirical formulas Eq. (13) are identified by applying the least-squares method for the averaged value of $\kappa_{40}(h_0, \mu_V, p_V, \mu_d, p_d)$ to every damper parameters $h_0, \mu_V, p_V, \mu_d, p_d$. Further details of Eq. (13) can be seen in reference [7].

$$\kappa_{40}(h_0, \mu_V, p_V, \mu_d, p_d) = \sqrt{1-h_{eq}^2}\left\{\left(A_1 + A_2 p_d + \frac{A_3}{p_d}\right)Log(\mu_d + 1.1) + \left(B_1 + B_2 p_d + \frac{B_3}{p_d}\right)Log(\mu_d - 0.9) + \left(C_1 + C_2 p_d + \frac{C_3}{p_d}\right)\right\} \quad (13)$$

2. 3 Seismic performance- based diagram

This section describes how to get the response performance-based diagram.
Now, Eq. (14) is obtained by substituting Eq. (11) into Eq. (12).

$$\left(\frac{\omega_0 x_{e,d}}{pS_{V,40}}\right) = \frac{\kappa_{40}(h_0, \mu_V, p_V, \mu_d, p_d)}{\sqrt{\{6(\mu_d - 1)(1 - p_d) + p_d(\mu_d^2 - 1) + 1\} + \frac{\pi 2 h_{eq} \mu_d^2}{\gamma}}} \quad (14)$$

$$\gamma = \frac{\omega_0}{\omega'} = \frac{T'}{T_E} \qquad h_{eq} = h_0\left[1 + \frac{2(1-p_V)}{\pi}\left\{\frac{\sqrt{\mu_V^2 - 1}}{\mu_V^2} - \cos^{-1}\left(\frac{1}{\mu_V}\right)\right\}\right]$$

Eq. (14) shows that specifying the parameters $h_0, \mu_V, p_V, \mu_d, p_d$, we can estimate the ratio $(\omega_0 x_{e,d} / pS_{V,40})$. Multiplying $(\mu_d \bullet (\omega'/\omega_0))$ to the ratio leads to the ratio (D_{max}/D_{40}), in which D_{max} is the maximum response displacement and D_{40} means the spectral displacement at the effective natural period T' in the design spectrum $pS_{V,40}$.

$$\left(\frac{D_{\max}}{D_{40}}\right) = \frac{\mu_d}{\gamma}\left(\frac{\omega_0 x_{e,d}}{pS_{V,40}}\right) \qquad (15)$$

The response velocity amplification is obtained as follows.
In the case of non-stationary vibration like earthquake ground motions, the maximum response velocity value does not agree with the value $\omega' \bullet D_{max}$, particularly over the long period range of a system with high viscous damping ratio.
Eq. (16) is defined accordingly as the equivalent circular frequency $\hat{\omega}_E$.

$$\hat{\omega}_E = \frac{V_{max}}{D_{max}} \qquad (16)$$

Fig. 6, for the 1940 El Centro N-S and the 1995 JR Takarazuka N-S records, shows the response velocity spectrum $S_{V,40}$, a set of $\hat{\omega}_E$ plotting the value of Eq. (16) and the ratio $(S_{V,40}/D_{40})$. As a result, the relationship expressed by Eq. (17) can be observed in engineering sense.

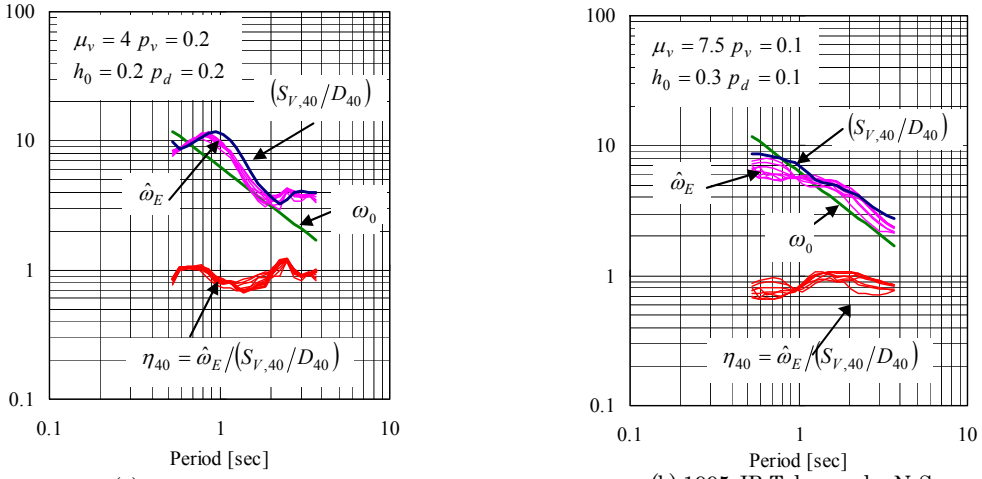

(a) 1940 El Centro N-S (b) 1995 JR Takarazuka N-S

Fig .6 Comparisons among $S_{V,40}$, $\hat{\omega}_E$, ω_0 and $\hat{\omega}_E/(S_{V,40}/D_{40})$

$$\eta_{40}(h_0, \mu_V, p_V, \mu_d, p_d) = \hat{\omega}_E \Big/ \left(\frac{S_{V,40}}{D_{40}}\right) \fallingdotseq \text{constant} \qquad (17)$$

In the same way, the numerical values of $\eta_{40}(h_0, \mu_V, p_V, \mu_d, p_d)$ are derived for all data of Table. 2. Applying the least-squares method, the constants in the empirical formulas Eq. (18) are identified for the averaged value of $\eta_{40}(h_0, \mu_V, p_V, \mu_d, p_d)$ for every damper parameters $h_0, \mu_V, p_V, \mu_d, p_d$. Further details of Eq. (18) can be seen in reference [7].
Finally, the relationships between the maximum displacement and the maximum velocity lead to Eq. (19).

$$\eta_{40}(h_0, \mu_V, p_V, \mu_d, p_d) = (R_1 \bullet p_d + R_2)/\mu_d + (S_1 \bullet p_d + S_2) \qquad (18)$$

$$\frac{V_{\max}}{S_{V,40}} = \eta_{40}\frac{D_{\max}}{D_{40}} \qquad (19)$$

The response absolute acceleration ratios can be derived as follows.
Suppose that the equivalent elastic system undergoes a harmonic vibration expressed by Eq. (20).

$$\left(\ddot{x}+\ddot{g}\right)=2h'_{eq}\omega'\dot{x}+\omega'^{2}x \qquad (20)$$

Using the knowledge that the equivalent damping ratio depends on the ratio of damping-energy loss per cycle to the strain energy stored at maximum displacement, the equivalent viscous damping ratio h'_{eq} can be expressed by Eq. (21).

$$h'_{eq}=\frac{E_d'+E_h'}{4\pi E_{eq,d}} \qquad (21)$$

$$E'_d=4\omega_0^2 {x_{e,d}}^2\left(1-p_d\right)\left(\mu_d-1\right)$$

$$E'_d=\pi 2h_0\omega_0 V_{\max}D_{\max}\left[1+\frac{2\left(1-p_V\right)}{\pi}\left\{\frac{\sqrt{\mu_V^2-1}}{\mu_V^2}-\cos^{-1}\left(\frac{1}{\mu_V}\right)\right\}\right] \qquad E_{eq,d}=\frac{1}{2}\left(\omega'\sqrt{1-h_{eq}^2}\right)^2 {D_{\max}}^2$$

Supposing a harmonic vibration, Eq. (20) can be rewritten as Eq. (22).
The maximum response acceleration ABS_{max} can be expressed by Eq. (23) through the root sum squares method. Making use of the relationships expressed by Eqs. (24) and (25), the relationships between ABS_{max}/A_{40} and D_{max}/D_{40} can be obtained by Eq. (26), in which A_{40} means the spectral acceleration at the effective period T' in the design spectrum $pS_{V,40}$

$$-\left(\ddot{x}+\ddot{g}\right)=2h'_{eq}\omega'\dot{x}+\omega'^{2}x=\omega'^{2}a\left(2h'_{eq}\cos\omega' t+\sin\omega' t\right) \qquad (22)$$

$$\left|\ddot{x}+\ddot{g}\right|_{\max}=\omega'^{2}a\sqrt{1+4{h'_{eq}}^2}\ \Rightarrow ABS_{\max}=A_{\max,d}\sqrt{1+4{h'_{eq}}^2} \qquad (23)$$

$$\left.\begin{aligned} A_{\max,d}&=\left\{1+p_d\left(\mu_d-1\right)\right\}A_{y,d} \qquad \left(\frac{A_{y,d}}{A_{40}}\right)=\gamma\left(\frac{\omega_0 x_{e,d}}{pS_{V,40}}\right)\\ \left(\frac{A_{\max,d}}{A_{40}}\right)&=\left(\frac{A_{y,d}}{A_{40}}\right)\left\{1+p_d\left(\mu_d-1\right)\right\}\end{aligned}\right\} \qquad (24)$$

$$A_{\max,d}=\frac{\gamma^2}{\mu_d}\left\{1+p_d\left(\mu_d-1\right)\right\}\left(\frac{D_{\max}}{D_{40}}\right)A_{40} \qquad (25)$$

$$\left(\frac{ABS_{\max}}{A_{40}}\right)=\frac{\gamma^2}{\mu_d}\left\{1+p_d\left(\mu_d-1\right)\right\}\sqrt{1+4{h'_{eq}}^2}\left(\frac{D_{\max}}{D_{40}}\right) \qquad (26)$$

3. ESTIMATION OF DAMPER PARAMETERS AND VERIFICATION BY TIME HISTORY ANALYSIS [7,8]

This section introduces the performance-based diagrams and the applying example for a preliminary design of a seismic isolation structure. The procedure is explained as follows.

Step 1:Set the design spectra for a given ground motion
Now, we adopt the time history named C3-JR TAKARAZUKA 1995 NS as the design earthquake ground motion, which is one of waves recorded in the 1995 Kobe earthquake. The peak values for the input are $\ddot{g}_{\max}=6.9m/s^2$ for acceleration, $\dot{g}_{\max}=0.86m/s$ for velocity and $g_{\max}=0.26m$ for displacement, respectively.
Fig. 7 indicates the design spectra ${}_pS_{V,40}$ and $S_{V,40}$. It can be easily realized that the configuration of ${}_pS_{V,40}$ extremely resembles the trapezoidal spectrum constructed with the peak values of $\ddot{g}_{\max}=6.9m/s^2$, $\dot{g}_{\max}=0.86m/s$ and $g_{\max}=0.26m$, respectively. This is the main reason that ${}_pS_{V,40}$ is adopted as the design spectrum.
Step 2: Specify the target response values
Specifying the values of damper parameters μ_V, p_V and p_d, respectively and reading the values of ${}_pS_{V,40}$ and $S_{V,40}$ at the effective natural period T', the performance based diagrams for the relations between $\left(ABS_{\max}/A_{40}\right)$

and $(D_{\max}/D_{40})$ can be constructed with the parameters μ_d and h_0 through from Eq.(13) to Eq.(26). Fig. 8 indicates one of the diagrams under the condition of $\mu_V = 3$, $p_V = 0.2$ and $p_d = 0.2$ for the secondary damper parameters and the values of ${}_pS_{V,40}$ and $S_{V,40}$ are $0.60m/s$ and $0.85m/s$ at the effective natural period $T' = 3.0s$ for the design spectra.

Now, we specify the target response values of the system under the above condition as follows.

$$ABS_{\max} = 1.3m/s^2 \qquad D_{\max} = 0.3m \qquad (27)$$

In order to obtain the target performance, the following conditions are required.

$$ABS_{\max} = 1.3m/s^2 = \left(\frac{ABS_{\max}}{A_{40}}\right)\cdot A_{40} \qquad D_{\max} = 0.3m = \left(\frac{D_{\max}}{D_{40}}\right)\cdot D_{40} \qquad (28)$$

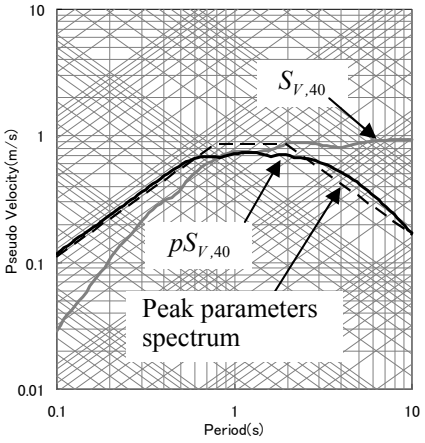

Fig .7 the spectra $S_{V,40}$ and $pS_{V,40}$ of the design earthquake motion of C3-JR Takarazuka 1995 N-S

The spectral values of A_{40} and D_{40} of ${}_pS_{V,40}$ at $T' = 3.0s$ can be read as $1.26m/s^2$ and $0.29m$, respectively. The requirement values for $(ABS_{\max}/A_{40})$ and $(D_{\max}/D_{40})$ become as follows.

$$\frac{ABS_{max}}{A_{40}} = \frac{1.3m/s^2}{1.26m/s^2} = 1.03 \qquad \frac{D_{max}}{D_{40}} = \frac{0.3m}{0.29m} = 1.03 \qquad (29)$$

Step 3 : Estimate the other damper parameters

The condition to satisfy Eq. (29) can be easily read as the ductility factor $\mu_d = 14.0$ and viscous damping ratio $h_0 = 0.30$ as shown in the broken lines of Fig. 8.

The elastic period T_E can be obtained by substituting $\mu_d = 14.0$ and $p_d = 0.2$ into Eq.(5) as follows.

$$\frac{T'}{T_E} = 1.68 \quad \rightarrow \quad T_E = \frac{3.0s}{1.68} = 1.79s \qquad (30)$$

The initial stiffness of the system with the condition of $m = 1{,}000ton$ becomes $k = 12{,}321kN/m$ and the yield deformation is decided accordingly by the relation of $x_{e,d} = D_{max}/\mu_d = 0.3m/14.0 = 0.021m$.

Fig.9 indicates the diagram of the relation between $(V_{\max}/S_{v,40})$ and $(D_{\max}/D_{40})$ under the same condition to Fig.8. From the above relation, we get $(V_{max}/S_{v,40}) = 0.99$. The relief velocity is decided by the equation $V_{y,h} = (V_{max}/\mu_v) = (V_{max}/S_{V,40}) \bullet S_{V,40} \bullet (1/\mu_V) = 0.99 \bullet 0.85/3 = 0.28m/s$.

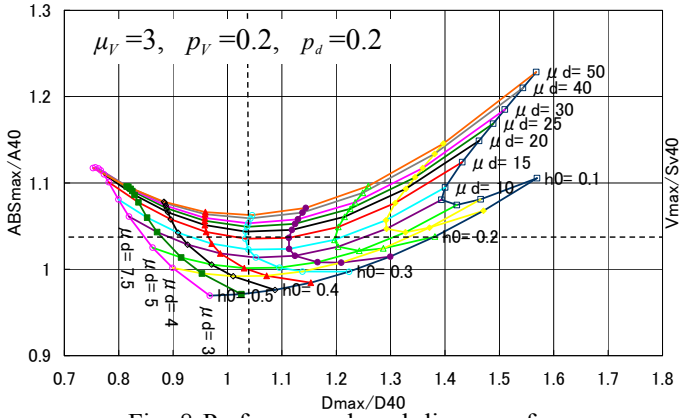

Fig .8 Performance-based diagrams for (ABS_{max}/A_{40}) and (D_{max}/D_{40})

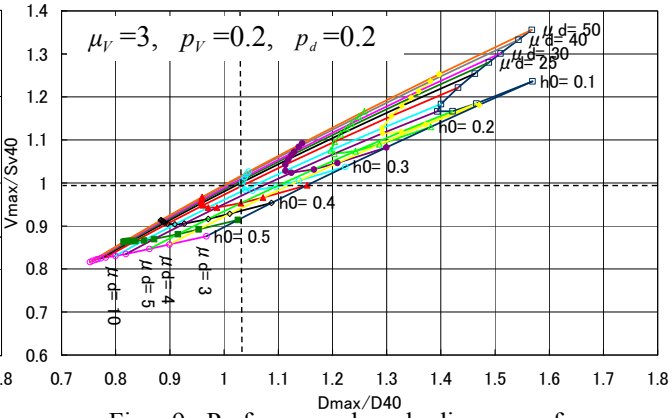

Fig .9 Performance-based diagrams for $(V_{max}/S_{V,40})$ and (D_{max}/D_{40})

Step 4 : Verify the accuracy of the estimated parameters.
Consequently, the estimated parameters of the system are arranged as follows.

$$m = 1000ton \quad k = 12{,}321kN/m \quad c = 2{,}106kN \cdot s/m \quad V_{y,h} = 0.28m/s \quad x_{ed} = 0.021m \quad p_d = 0.2 \quad p_V = 0.2$$
$$target \ \ response \ \ values \ \ D_{max} = 0.3m(\mu_d = 14) \quad V_{max} = 0.84m/s(\mu_V = 3) \quad ABS_{max} = 1.3m/s^2$$

Table 3 shows the comparison between the estimation values and the result obtained by the inelastic time history analysis. It shows that the estimated values have enough accuracy in applying the preliminary seismic design.

Table 3. Comparisons between the values estimated by the performance-based diagrams and the values analyzed by time history analysis

	Estimation values	Analysis values	Estimate value/ Analysis value
Absolute acceleration	1.30 m/s^2	1.53 m/s^2	0.85
Velocity	0.84 m/s	0.87 m/s	0.97
Displacement	0.30 m	0.31 m	0.97
Yield deformation	0.021 m	-	-
ductility factor	14.0	14.5	0.97
relief velocity	0.26 m/s	-	-
relief velocity ratio	3.0	3.1	0.97

4. CONCLUSION

This paper introduced an inverse design method for SDOF structures through performance-based diagrams which can easily estimate suitable design parameters for various dampers in order to satisfy the target design performances to be specified for a given earthquake ground motion.
The accuracy of the estimated parameters including other systems is also verified by a number of time history simulations. The result shows that the proposed method has enough accuracy in applying preliminary seismic designs. Needless to say, the diagrams can be utilized to evaluate the response values for a given ground motion after specifying the effective natural period and the damper parameters including the target ductility factor and the viscous damping ratio.

ACKNOWLEGEMENTS

This research was conducted as a part of the Study on Environmentally Sustainable and Disaster Resistant Cities, headed by Prof. Shinji Ishimaru, commenced under the “Academic Frontier Promotion Program (College of Science and Technology, Nihon University: continuous study) of Ministry of Education, Calture, Sports, Science and Technology.

REFERENCES

[1] Kasai, K. and Kawanabe, Y. (2005). Equivalent linearization to predict dynamic properties and seismic peak responses of a structural system with high viscous damping and hysteretic damping. *J. Struct. Constr.Eng., AIJ*, No.591, 43-51., JPN
[2] Akiyama, H. (1999). Earthquake-Resistant design method for buildings based on energy balance. *Gihodo*, JPN.
[3] Higashino, S. and Kitamura, H. (2005). Energy-balance based seismic response prediction methods for seismic isolated buildings with rubber bearing and viscous dampers. *J. Struct. Constr.Eng., AIJ*, No.588, 79-86., JPN
[4] Ishimaru, S. (2004). Introduction of seismic response control design. *Syokokusya*., JPN
[5] Ishimaru, S. (1996). Seismic performance design by separated variables of energy spectrum. *Microcomputers in Civil Engineering*, 11, 343-354.
[6] Kasai, K. and Nishimura, T. (2004). Equivalent Linearization of passive control system with oil damper bilinearly dependent on velocity. *J. Struct. Constr.Eng., AIJ*, No.583, 47-54., JPN
[7] Hata, I., Ishimaru, S. and Hasegawa, J. (2007). On performance based design method for systems with non-linear viscous damper and elasto-plastic damper. *J. Struct. Constr.Eng., AIJ*, No.617, 47-54., JPN
[8] Ishimaru, S. (2008). Dynamic Design Method on basis of Response Control. *Kenchiku-gijutu.*, JPN